arXiv:hep-ph/9805293v1 12 May 1998

BARI-TH/299-98

# Vacuum oscillations and variations of solar neutrino rates in SuperKamiokande and Borexino

B. Faïd,[a] G. L. Fogli,[b] E. Lisi,[b] and D. Montanino [b]
[a] *Institut de Physique, Université des Sciences et de la Technologie, DZ-16111 Algiers, Algeria*
[b] *Dipartimento di Fisica and Sezione INFN di Bari, Via Amendola 173, I-70126 Bari, Italy*

## Abstract

The vacuum oscillation solution to the solar neutrino problem predicts characteristics variations of the observable neutrinos rates, as a result of the $L/E_\nu$ dependence of the $\nu_e$ survival probability ($L$ and $E_\nu$ being the neutrino pathlength and energy, respectively). The $E_\nu$-dependence can be studied through distortions of the recoil electron spectrum in the SuperKamiokande experiment. The $L$-dependence can be investigated through a Fourier analysis of the signal in the SuperKamiokande and Borexino experiments. We discuss in detail the interplay among such observable variations of the signal, and show how they can help to test and constrain the vacuum oscillation solution(s). The analysis includes the 374-day SuperKamiokande data.

PACS number(s): 26.65.+t, 13.15.+g, 14.60.Pq

Typeset using REVTEX

## I. INTRODUCTION

Neutrino flavor oscillations [1] with wavelength comparable to the Earth-Sun distance [2] represent a solution [3] to the deficit of solar $\nu$'s [4] observed in the four pioneering underground experiments Homestake [5], Kamiokande [6], SAGE [7], and GALLEX [8], as compared to the standard solar model predictions [9]. The recent SuperKamiokande data [10] confirm the deficit, and can be interpreted within the vacuum oscillation hypothesis as well [11,12]. The planned Borexino solar neutrino experiment [13,14] (in construction), designed to detect monochromatic $^7$Be neutrinos ($E_\nu = 0.86$ MeV), is expected to test this hypothesis with unprecedented sensitivity [15–17].

An update of the current neutrino flux measurements [6,10,18–20] is given in Table I. Figure 1 shows our vacuum oscillation fit to the data of Table I, as obtained from a $\chi^2$ analysis (including solar model uncertainties as in [21]). We have assumed, for simplicity, two neutrino families. It can be seen that four regions (A, B, C, and D) are allowed at 95% C.L., the absolute minimum being located within the solution B ($\chi^2_{\rm min} = 3.4$ and $N_{\rm DF} = 3 = 5 - 2$).

Various tests can be envisaged to discriminate among the four solutions in Fig. 1. In particular, since the neutrino oscillation length is proportional to the pathlength-to-energy ratio $L/E_\nu$, deviations of event distributions from the expected shape in either $L$ or $E_\nu$ (or related parameters) represent direct tests of neutrino vacuum oscillations (see, e.g., [22–24]). It turns out that, in general, SuperKamiokande is more (less) sensitive than Borexino to $E_\nu$-related ($L$-related) spectral shape deviations; therefore, the two experiments provide complementary tools to study the vacuum oscillation hypothesis. The purpose of this work is to investigate in detail the tests of the vacuum oscillation hypothesis that can be performed at SuperKamiokande and Borexino, and their interplay. The results will be shown in a form that makes easy to derive the experimental accuracy needed to perform a specific test.

The plan of this paper is as follows. In Sec. II we discuss the tests of energy spectra deviations, in the light of the recent SuperKamiokande results. In Sec. III we discuss in detail the Fourier analysis of the signal, building upon our previous work [25]. In Sec. III we apply these tests to SuperKamiokande and Borexino, both separately and jointly. In Sec. IV we draw our conclusions. Some technical aspects of our analysis are described in the Appendix.

## II. $E_\nu$-RELATED TESTS: AVERAGE ELECTRON KINETIC ENERGY

Both SuperKamiokande and Borexino can measure the energy spectrum of recoil electrons from neutrino scattering. The standard (i.e., no oscillation) SuperKamiokande spectrum can be found in Fig. 4 of Ref. [11]. For completeness, we show in Fig. 2 the standard electron energy spectrum in Borexino (details about the inclusion of energy threshold and resolution effects are given in the Appendix). The main contribution to the spectrum in Fig. 2 is given by the 0.86 MeV $^7$Be line, which is responsible for the Compton edge at $\sim 0.66$ MeV. The edge is smeared by the finite energy resolution. The rise at low energies is due to *pp* neutrinos, while the tail at high energies is basically due to CNO neutrinos. The prospective analysis window is also indicated in Fig. 2. The standard neutrino fluxes have been taken from [9].

Distortions of the neutrino energy spectrum due to oscillations are generally reflected (although somewhat degraded) in the electron energy spectrum. An effective parametrization of such distortions is given by the fractional variation of the average kinetic energy $\langle T\rangle$ of the electron, an approach extensively developed in [22] and applied to the SuperKamiokande data in [11,26]. In particular, the analysis [26] of the most recent (374 day) measurements of the electron spectrum in SuperKamiokande [10,27–31] gives a fractional deviation

$$\frac{\Delta\langle T\rangle}{\langle T\rangle}\times 100 = 0.95 \pm 0.73\ . \tag{1}$$

Such deviation is consistent with zero (no oscillation) at the level of $1.2\sigma$, and disfavors scenarios predicting negative values for $\Delta\langle T\rangle/\langle T\rangle$.

Concerning Borexino, the expected *shape* variations of the energy distribution are very small, since the main contribution to the electron spectrum comes from a monoenergetic source of neutrinos ($^7$Be), rather than from a continuous source as in SuperKamiokande ($^8$B). Neutrino oscillations are expected to change significantly the global Borexino rate but not its energy spectrum.

## III. $L$-RELATED TESTS: FOURIER EXPANSION OF THE SIGNAL

The variations of the solar neutrino pathlength $L$ due to the eccentricity of the Earth orbit produce a geometrical ($1/L^2$) modulation of the neutrino flux. Additional semiannual modulations are expected in the presence of neutrino oscillations [32]. The Fourier analysis of the measured flux represents an effective tool to study both kinds of $L$-related modulations [25].

In this Section we outline the Fourier analysis of the signal observable in solar neutrino experiments. In the first three subsections, we describe the general formalism and the results for the "no oscillation" and "$2\nu$ oscillation" cases (see also Ref. [25] for further details). In the last two subsections we generalize the analysis to $3\nu$ oscillations and then discuss a useful check of both the symmetry properties and the estimated uncertainties of the signal.

### A. General formalism

The Earth orbit radius, $L$, varies periodically in time ($t$) around its average value, $L_0 = 1.496\times 10^8$ km, according to

$$L(t) = L_0\left(1-\varepsilon\,\cos\frac{2\,\pi\,t}{T}\right) + O(\varepsilon^2)\ , \tag{2}$$

where $\varepsilon = 0.0167$ is the orbit eccentricity and $T = 1$ yr ($t = 0$ at the perihelion). Terms of $O(\varepsilon^2)$ or higher are negligible for our purposes.

The neutrino signal $S$ is also, in general, a periodic function. Assuming a constant background $B$, the total observed neutrino rate $R$ is:

$$R(t) = B + S(t)\ . \tag{3}$$

For symmetry reasons, the analysis can be restricted to the time interval $[0, T/2]$.[1] It is understood that events collected in subsequent half-years must be symmetrically folded in this interval. The data sample consists then of $N$ events collected at different times $\{t_i\}_{1\leq i\leq N}$, with $t_i \in [0,\, T/2]$ and $N$ equal to the total sum of background and signal events, $N = N_S + N_B$. Notice that, in general, one can determine $N_B$ and $N_S$ but cannot distinguish background and signal on an event-by-event basis.

The expansion of the signal in terms of Fourier components $f_n$ reads

$$S(t) = S\left(1 + 2\sum_{n=1}^{\infty} f_n \cos\frac{2\pi n t}{T}\right)\ , \tag{4}$$

where $S$ is the time-averaged signal

$$S = \frac{2}{T}\int_0^{T/2} dt\, S(t)\ . \tag{5}$$

The $n$-th harmonic corresponds to a period of $1/n$ yr. The explicit form of $f_n$ reads

$$\begin{aligned} f_n &= \frac{2}{ST}\int_0^{T/2} dt\, R(t)\cos\frac{2\pi n t}{T} && (6)\\ &= \frac{1}{N_S}\sum_{i=1}^{N_S+N_B}\cos\frac{2\pi n t_i}{T} \qquad (0 \leq t_i \leq T/2)\ , && (7) \end{aligned}$$

where Eqs. (6) and (7) represent the theoretical definition and the experimental determination of the $f_n$'s, respectively [25].

Assuming purely statistical fluctuations of the signal and of the background, the variance of the $f_n$'s reads:

$$\mathrm{var}(f_n) = \frac{1 + f_{2n} + N_B/N_S}{2\, N_S}\ . \tag{8}$$

It turns out that the values of the $f_{2n}$'s are $\ll 1$ in all cases of practical interest. Therefore, to a good approximation, the one-sigma statistical error $\sigma_f = \sqrt{\mathrm{var}(f_n)}$ affecting $f_n$ is given by

$$\sigma_f \simeq \sqrt{\frac{N_S + N_B}{2\, N_S^2}} \tag{9}$$

for *any* $n$. The correlations between the statistical errors of different harmonics are also negligible [25].

Finally, the general expression of the signal $S$ expected in the presence of oscillations is

---

[1] Experimental tests of the symmetry properties of the signal are discussed at the end of this section.

$$S^{\rm osc}(t) \propto \frac{L_0^2}{L^2(t)} \int dE\, \lambda(E) \left[\sigma_e(E) P(E,t) + \sigma_x(E)(1 - P(E,t))\right] , \tag{10}$$

where $E$ is the neutrino energy, $\lambda$ is the neutrino energy spectrum, $\sigma_e$ ($\sigma_x$) is the $\nu_e$ ($\nu_x$, $x = \mu$, $\tau$) interaction cross section, and $P$ is the $\nu_e$ survival probability, which varies in time through $L(t)$ [32]. It is understood that the cross sections $\sigma_{e,x}$ must be corrected for energy threshold and resolution effects, as described in the Appendix.

### B. Standard (no oscillation) case

In the standard (no oscillation) case, characterized by $P(E,t) = 1$, the signal $S$ varies as $S^{\rm std}(t) \propto L^{-2}(t)$. The standard Fourier components are simply given by

$$f_n^{\rm std} = \varepsilon \delta_{n1} \ , \tag{11}$$

i.e., only the first harmonic is nonzero and measures the Earth's orbit eccentricity.

### C. $2\,\nu$ oscillation case

In this case, $\nu_e$ is a linear combination of two mass eigenstates ($\nu_1$, $\nu_2$) characterized by a mixing angle $\theta$

$$\nu_e = \cos\theta\, \nu_1 + \sin\theta\, \nu_2 \tag{12}$$

and by a squared mass difference $\delta m^2$,

$$\delta m^2 = |m_2^2 - m_1^2| \ . \tag{13}$$

The corresponding $\nu_e$ survival probability is given by

$$P^{2\nu}(E,t) = 1 - \frac{1}{2} \sin^2 2\theta \left(1 - \cos \frac{\delta m^2\, L(t)}{2\, E}\right) \ . \tag{14}$$

The Fourier components can be cast in the following, compact form [25]:

$$f_n^{2\nu} = \frac{\varepsilon \delta_{n1} - \sin^2 2\theta\, D_n(\delta m^2)}{1 - \sin^2 2\theta\, D_0(\delta m^2)} \tag{15}$$

where the (detector-dependent) functions $D_n$ are given by

$$D_n(\delta m^2) = \frac{\displaystyle\int dE\, \lambda\, (\sigma_e - \sigma_x)\, U_n}{\displaystyle 2 \int dE\, \lambda\, \sigma_e} \quad (n \geq 0) \tag{16}$$

and the universal (i.e., detector-independent) functions $U_n$ are given by

$$U_n(z) = \delta_{n0} - u_n(z) - \varepsilon [u_{n+1}(z) + u_{n-1}(z) - \delta_{n1}] \ ,$$
$$u_n(z) = \cos\left(z - \frac{n\pi}{2}\right) J_n(\varepsilon z) \ ,$$

where $z = \delta m^2 L_0 / 2E$ and $J_n$ is the Bessel function of order $n$. Notice that, although our calculations are of $\mathcal{O}(\varepsilon)$, all orders in $\varepsilon z$ are kept, since $z$ may be large.

### D. $3\nu$ oscillation case

In this case, $\nu_e$ is a linear combination of three mass eigenstates ($\nu_1$, $\nu_2$, $\nu_3$), usually parametrized in one of the following two forms:

$$\begin{aligned} \nu_e &= U_{e1}\,\nu_1 + U_{e2}\,\nu_2 + U_{e3}\,\nu_3 && (17)\\ &= c_\phi(c_\omega\,\nu_1 + s_\omega\,\nu_2) + s_\phi\,\nu_3\ , && (18)\end{aligned}$$

where $s = \sin$, $c = \cos$, and $U^2_{e1} + U^2_{e2} + U^2_{e3} = 1$ (see, e.g., [23]). In addition, we assume a hierarchy of mass differences:

$$\delta m^2 \ll |m^2_3 - m^2_{1,2}|\ . \tag{19}$$

The hypothesis (19) covers most of the situations of phenomenological interest [33]. In this case, the $3\nu$ oscillation probability is given by

$$\begin{aligned} P^{3\nu}(E,t) &= 1 - 2\,U^2_{e3}(1-U^2_{e3}) - 2\,U^2_{e1}U^2_{e2}\left(1 - \cos\frac{\delta m^2\,L(t)}{2\,E}\right) && (20)\\ &= c^4_\phi\,P^{2\nu}(E,t)\Big|_{\theta\to\omega} + s^4_\phi\ . && (21)\end{aligned}$$

We have worked out the corresponding Fourier components, which read:

$$\begin{aligned} f^{3\nu}_n &= \frac{\varepsilon\,\delta_{n1}[1 - 4\,U^2_{e3}(1-U^2_{e3})\,r] - 4\,U^2_{e1}U^2_{e2}\,D_n(\delta m^2)}{1 - 4\,U^2_{e3}(1-U^2_{e3})\,r - 4\,U^2_{e1}U^2_{e2}\,D_0(\delta m^2)} && (22)\\ &= \frac{\varepsilon\,\delta_{n1}(1 - s^2_{2\phi}r) - s^2_{2\omega}c^4_\phi\,D_n(\delta m^2)}{1 - s^2_{2\phi}r - s^2_{2\omega}c^4_\phi D_0(\delta m^2)} && (23)\end{aligned}$$

where the functions $D_n$ are defined in Eq. (16) and

$$r = \frac{\displaystyle\int dE\,\lambda(\sigma_e - \sigma_x)}{2\displaystyle\int dE\,\lambda\sigma_e}\ . \tag{24}$$

Notice that $f^{3\nu} \to f^{2\nu}$ for $U_{e3}(= s_\phi) \to 0$, as it should.

### E. A useful consistency check

*A priori*, the signal $S(t)$ must obey the symmetry $S(t) = S(T-t)$ in the one-year interval $[0,\,T]$ (either with or without oscillations). We have made use of this property in Eqs. (5–7). The experimental test of such symmetry property is not without merit, since its failure might signal systematic, time-dependent effects, such as unexpected variations of the detection efficiency or of the background level. Within our approach, this is equivalent to check that the "sine" Fourier components $g_n$, defined as

$$g_n = \frac{1}{N_S}\sum_{i=1}^{N_S+N_B}\sin\frac{2\pi n t_i}{T} \qquad (0 \le t_i \le T)\ , \tag{25}$$

are identically zero, as they should (both in the standard case and in the presence of possible oscillations):

$$g_n^{\rm std} = g_n^{\rm osc} = 0\ . \tag{26}$$

Notice that, in Eq. (25), the event "arrival times" are folded in the interval $[0,\, T]$ and not in $[0,\, T/2]$.

The experimentally inferred $g_n$'s will be distributed around zero with a variance $\mathrm{var}(g_n)$. As far as statistical fluctuations are concerned, the calculation of $\mathrm{var}(g_n)$ is analogous to $\mathrm{var}(f_n)$ [25] and gives:

$$\mathrm{var}(g_n) = \frac{1 - f_{2n} + N_B/N_S}{2\, N_S}\ . \tag{27}$$

However, as already noticed, the $f_{2n}$'s are generally $\ll 1$ and thus can be neglected in the above equation. Therefore, the statistical uncertainty $\sigma_g = \sqrt{\mathrm{var}(g_n)}$ is approximately equal for all the $g_n$'s and has the same expression as $\sigma_f$ [Eq. (9)].

In conclusion, it is useful to check that the semiannual variations of the solar neutrino signal are indeed symmetric in time. This implies that the "sine" Fourier components $g_n$ defined in Eq. (25) should form a distribution with mean value $\langle g_n\rangle = 0$ and standard deviation $\sigma_g = \sqrt{(N_S + N_B)/2N_S^2}$. This test is universal, i.e. it is valid with or without oscillation effects. Any deviation of the mean and variance of the $g_n$ distribution from their standard values (0 and $\sigma_g^2$, respectively) would indicate the presence (and the magnitude) of systematic effects beyond the purely statistical fluctuations of either the background or the signal. These effects (if any) should then be accounted for by the experimentalists, before performing an unbiased analysis of the time variations of the signal.

## IV. VACUUM OSCILLATION TESTS AT SUPERKAMIOKANDE AND BOREXINO

In this section we analyze the tests of the vacuum oscillation hypothesis that can be performed at SuperKamiokande and Borexino, both separately and jointly. We consider two observables for each experiment. In particular, we analyze $\Delta\langle T\rangle/\langle T\rangle$ and $f_1 - \varepsilon$ for SuperKamiokande (SK), and $f_1 - \varepsilon$ and $f_2$ for Borexino (BX):

$$\text{Observables} \left\{ \begin{array}{l} \Delta\langle T\rangle/\langle T\rangle \text{ and } f_1^{\rm SK} - \varepsilon \quad \text{(SuperKamiokande)}\ , \\ f_1^{\rm BX} - \varepsilon \text{ and } f_2^{\rm BX} \quad \text{(Borexino)}\ . \end{array} \right. \tag{28}$$

All the above variables are zero in the standard (no oscillation) case. In the oscillation range of interest, Fourier components with $n > 1$ ($n > 2$) are not relevant for SuperKamiokande (Borexino) [25]. For simplicity, we will consider only $2\nu$ oscillations, and the corresponding preferred regions A, B, C, and D of Fig. 1.

### A. Tests at SuperKamiokande

Figure 3 shows the four solutions A, B, C, and D (gray regions) and the no oscillation point (star) in the plane charted by the parameters $\Delta\langle T\rangle/\langle T\rangle$ (the fractional deviation of the mean electron kinetic energy) and $f_1^{\rm SK}-\varepsilon$ (the deviation of the first Fourier component from its standard value). Also shown is the horizontal band allowed at $\pm 1\sigma$ by the $\Delta\langle T\rangle/\langle T\rangle$ datum of Eq. (1).

Figure 3 evidences that solutions C and D (which predict large, negative values for $\Delta\langle T\rangle/\langle T\rangle$) are highly disfavored by the SuperKamiokande measurement of Eq. (1). In particular, solution C is disfavored at $> 4\sigma$ and solution D at $> 6\sigma$. On the other hand, the datum of Eq. (1) is unable to discriminate among the solutions A, B, and the no oscillation point at the $2\sigma$ level, although solution A seems to be preferred. We can summarize these findings by saying that, under the hypothesis of $2\nu$ oscillations, the *combined* data of Table I and Eq. (1) select the solutions A and B in Fig. 1, corresponding to the following approximate ranges (at 95% C.L.) for the neutrino mass-mixing parameters:

$$0.59 \lesssim \delta m^2 \lesssim 0.84\ (\times 10^{-10}\ {\rm eV}^2)\ , \tag{29}$$

$$0.66 \lesssim \sin^2 2\theta \lesssim 1\qquad\qquad . \tag{30}$$

Notice that the spread of the above parameters is only about ±20%. Also notice that $2\nu$ maximal mixing ($\sin^2 2\theta = 1$) is allowed only in a restricted range of $\delta m^2$ ($\sim 0.59$–$0.61\times 10^{-10}$ eV$^2$).

Concerning $f_1$, we cannot infer its value from the limited data which are publicly available [10,27–31]. At any rate, the estimated uncertainty $\sigma_f$ of $f_1$ [see Eq. (9)] for $\sim 1$ yr of data taking is about $\pm 0.02$ [11]—too large to discriminate any of the solutions A, B, C, and D. Significantly higher statistics are needed to reduce such error.

An interesting feature of Fig. 3 is the tight correlation between the variables $f_1-\varepsilon$ and $\Delta\langle T\rangle/\langle T\rangle$, which parametrize $L$-related and $E_\nu$-related spectral distortions, respectively. Such correlation can be traced to the $L/E_\nu$ dependence of the oscillation probability, as emphasized in [24]. One can use such correlation to "predict" the value of $f_1-\varepsilon$ in SuperKamiokande for a given value of $\Delta\langle T\rangle/\langle T\rangle$ in Eq. (1). More precisely, from Fig. 3 one derives that the values of $f_1-\varepsilon$ compatible with both the horizontal band and the solution A should lie in the range $\sim 0.005$–$0.01$. In other words, one expects an enhancement of the semiannual modulations of the neutrino flux (relatively to the purely geometrical one) in the range $[0.005/\varepsilon,\ 0.01/\varepsilon] = 30$–$60\%$ at $\sim 1\sigma$. This is a clear prediction that needs, however, several years of data taking at SuperKamiokande to be tested.

### B. Tests at Borexino

Figure 4 shows the four solutions A, B, C, and D (gray regions) in the plane charted by the parameters $f_1^{\rm BX}-\varepsilon$ and $f_2^{\rm BX}$ (the deviation of the first two Fourier components from their standard values). The no oscillation point (star) corresponds to the origin.

The amplitude of the second harmonic appears to be generally smaller than the first; nevertheless, both should be detectable in a sample of a few thousand events. E.g., for

$N_S \simeq N_B \simeq 5000$ events, the expected statistical error of $f_1$ and $f_2$ is only about $\pm 0.014$ [see Eq. (9)], ensuring clear detection of semiannual modulations (provided that systematics do not dominate the error budget). However, the four solutions A, B, C, D are rather close to each other in the Fourier parameter space, and it might be difficult to distinguish among them using only these two variables.

By comparing Figs. 3 and 4, it can be noticed that the solutions A and B (currently favored by SuperKamiokande data) predict rather different values for the first Fourier harmonic in SuperKamiokande and Borexino, as a result of the different energy ranges probed by these two experiments. In particular, within solution A it is always $f_1^{\rm SK} - \varepsilon > 0$, while $f_1^{\rm BX} - \varepsilon$ can be either positive or negative. Therefore, at present the sign of the semiannual variations in Borexino is unpredictable.

It is interesting to notice that, both in $2\nu$ and $3\nu$ oscillations, the Fourier component ratio $f_2/(f_1 - \varepsilon)$ depends only on $\delta m^2$ and not on the mixing angle(s) [see Eqs. (15) and (23)]. Therefore, such ratio can constrain the value of $\delta m^2$ in a model-independent way.

### C. Combination of SuperKamiokande and Borexino tests

Figure 5 shows the four solutions A, B, C, and D (gray regions) in the four planes charted by the Borexino observables $f_1^{\rm BX} - \varepsilon$ and $f_2^{\rm BX}$ ($x$-axes) and by the SuperKamiokande observables $f_1^{\rm SK} - \varepsilon$ and $\Delta\langle T\rangle/\langle T\rangle$ ($y$-axes). Also shown is the horizontal band allowed at $\pm 1\sigma$ by the $\Delta\langle T\rangle/\langle T\rangle$ datum of Eq. (1). Within such band, the values of $f_1^{\rm BX} - \varepsilon$ (as well as those of $f_2^{\rm BX}$) can be either positive or negative, as observed in the previous subsection. Figure 5 shows that the present indeterminacy in the sign of $f_1^{\rm BX} - \varepsilon$ cannot be resolved by increasing the accuracy of the SuperKamiokande data.

The similarity between the upper and lower panels in Fig. 5 is due to the tight correlation between the SuperKamiokande variables $f_1^{\rm SK} - \varepsilon$ and $\Delta\langle T\rangle/\langle T\rangle$. This similarity should be reflected in the experimental data, if vacuum oscillations indeed occur. When experimental data will be available for all the four observables charting the panels in Fig. 5, one of the four solutions should be easily spotted in at least one of the four panels. However, in the unlucky situation of data points close to the no oscillation case, it might be difficult to distinguish between such case and solution B. The possibility to separate the no oscillation point from solution B would then depend decisively on the reduction of the $\Delta\langle T\rangle/\langle T\rangle$ uncertainty (see upper panels of Fig. 5). In any case, the reader can judge the discriminating power of the two experiments by drawing prospective data points and error bars in each panel of Fig. 5.

## V. SUMMARY AND CONCLUSIONS

We have studied tests of vacuum oscillations of solar neutrinos in the SuperKamiokande and Borexino experiments, both separately and jointly. The tests are sensitive to either energy or time variations of the neutrino flux. The interplay between such tests has been investigated, in the light of the most recent data (374 day) from the SuperKamiokande experiment. The results have been displayed in a graphical form (Figs. 3–5) that allows to determine easily the experimental accuracy needed to test the vacuum oscillation solution(s). We have found that: (i) The total neutrino rates measured by solar $\nu$ experiments can be fitted in four distinct regions of the mass-mixing parameter space; (*ii*) Two of the four solutions are strongly disfavored by the SuperKamiokande energy spectrum data; (*iii*) The energy spectrum data do not discriminate significantly (at present) the remaining two solutions between them and from the no oscillation case; (*iv*) The amplitude of semiannual variations of the solar $\nu$ flux in SuperKamiokande is predicted to be about 30–60% in excess of the purely geometric one (at $1\sigma$); (*v*) The sign of semiannual variations (due to oscillations) in Borexino is not determined by present data; (*vi*) The *joint* information coming from the energy spectrum data (SuperKamiokande) and from the Fourier transform of the solar neutrino rates (SuperKamiokande, Borexino) can provide powerful tests of the vacuum oscillation solutions. Besides, we have generalized the Fourier transform formalism to three-flavor oscillations, and we have discussed a useful check of the time symmetry of the signal.

## ACKNOWLEDGMENTS

We are grateful to J. G. Learned for useful discussions and helpful suggestions. EL thanks the Centro de Física das Interacções Fundamentais at the Instituto Superior Técnico of the University of Lisbon, Portugal, for kind hospitality during the preparation of this work. BF thanks the Dipartimento di Fisica of Bari, Italy, for hospitality.

## APPENDIX: ENERGY THRESHOLD AND RESOLUTION EFFECTS

In the calculation of the expected signal [Eq. (10)], it is understood that the $\nu_\alpha$-$e$ cross sections $\sigma_\alpha(E)$ ($\alpha = e,\, x$) have to be properly corrected to take into account the detector energy resolution and the analysis window for each experiment. Here we give some details about such corrections.

Both in Borexino and in SuperKamiokande, the finite energy resolution due to the photon statistics implies that the *measured* kinetic energy $T$ of the scattered electron is distributed around the *true* kinetic energy $T'$ according to a resolution function $R(T,\, T')$ of the form [22]:

$$R(T,\, T') = \frac{1}{\sqrt{2\pi}s} \exp\left[-\frac{(T-T')^2}{2s^2}\right] \ , \tag{A1}$$

where

$$s = s_0\sqrt{T'/\mathrm{MeV}} \ , \tag{A2}$$

and $s_0 = 57.7$ KeV and 0.47 MeV for Borexino [15] and SuperKamiokande [10,11], respectively. On the other hand, the distribution of the true kinetic energy $T'$ for an interacting neutrino of energy $E_\nu$ is dictated by the differential cross section $d\sigma_\alpha(E_\nu,\, T')/dT'$, that we take from [34]. The kinematic limits are:

$$0 \leq T' \leq \overline{T}'(E_\nu) \ , \ \ \overline{T}'(E_\nu) = \frac{E_\nu}{1 + m_e/2E_\nu} \ . \tag{A3}$$

Concerning the measured kinetic energy, the present analysis window for SuperKamiokande is $[T_{\rm min},\, T_{\rm max}] = [6.5\ {\rm MeV} - m_e,\, 20\ {\rm MeV} - m_e]$. The prospective analysis window for Borexino (as used in this paper) is [0.25, 0.8] MeV.

For assigned values of $s_0$, $T_{\rm min}$, and $T_{\rm max}$, the corrected cross section $\sigma_\alpha(E_\nu)$ is defined as:

$$\sigma_\alpha(E_\nu) = \int_{T_{\rm min}}^{T_{\rm max}} dT \int_0^{\overline{T}'(E_\nu)} dT'\, R(T,\, T')\, \frac{d\sigma_\alpha(E_\nu,\, T')}{dT'}\ . \tag{A4}$$

It is useful to reorder the integrands, obtaining

$$\sigma_\alpha(E_\nu) = \int_0^{\overline{T}'(E_\nu)} dT'\, W(T')\, \frac{d\sigma_\alpha(E_\nu,\, T')}{dT'}\ , \tag{A5}$$

where the function $W(T')$, which embeds the detector specifications $s_0$, $T_{\rm min}$, and $T_{\rm max}$, is given by

$$W(T') = \frac{1}{2}\left[ {\rm erf}\left(\frac{T_{\rm max} - T'}{\sqrt{2}\, s}\right) - {\rm erf}\left(\frac{T_{\rm min} - T'}{\sqrt{2}\, s}\right)\right]\ , \tag{A6}$$

with $s$ as in Eq. (A2) and

$${\rm erf}(x) = \frac{2}{\sqrt{\pi}} \int_0^x dt\, e^{-t^2}\ . \tag{A7}$$

# TABLES

TABLE I. Neutrino event rates measured by solar neutrino experiments, and corresponding predictions from the standard solar model [9]. The quoted errors are at $1\sigma$.

| Experiment | Ref. | Data ±(stat.) ±(syst.) | Theory [9] | Units |
|---|---|---|---|---|
| Homestake | [18] | $2.56 \pm 0.16 \pm 0.15$ | $9.3^{+1.2}_{-1.4}$ | SNU |
| Kamiokande | [6] | $2.80 \pm 0.19 \pm 0.33$ | $6.62^{+0.93}_{-1.12}$ | $10^6$ cm$^{-2}$s$^{-1}$ |
| SAGE | [19] | $69.9^{+8.5+3.9}_{-7.7-4.1}$ | $137^{+8}_{-7}$ | SNU |
| GALLEX | [20] | $76.4 \pm 6.3^{+4.5}_{-4.9}$ | $137^{+8}_{-7}$ | SNU |
| SuperKam. | [10] | $2.37^{+0.06+0.09}_{-0.05-0.06}$ | $6.62^{+0.93}_{-1.12}$ | $10^6$ cm$^{-2}$s$^{-1}$ |

# REFERENCES

[1] B. Pontecorvo, Zh. Eksp. Teor. Fiz. **53**, 1717 (1967) [Sov. Phys. JETP **26**, 984 (1968)]; V. Gribov and B. Pontecorvo, Phys. Lett. **28B**, 493 (1969).

[2] S. L. Glashow and L. M. Krauss, Phys. Lett. B **190**, 199 (1987).

[3] P. I. Krastev and S. T. Petcov, Phys. Rev. D **53**, 1665 (1996).

[4] J. N. Bahcall, *Neutrino Astrophysics* (Cambridge University Press, Cambridge, England, 1989).

[5] R. Davis (Homestake Collaboration), Prog. Part. Nucl. Phys. **32**, 13 (1994).

[6] Y. Fukuda *et al.* (Kamiokande Collaboration), Phys. Rev. Lett. **77**, 1683 (1996).

[7] J. N. Abdurashitov *et al.* (SAGE Collaboration), Phys. Rev. Lett. **77**, 4708 (1996).

[8] W. Hampel *et al.* (GALLEX Collaboration), **288**, 384 (1996).

[9] J. N. Bahcall and M. H. Pinsonneault, Rev. Mod. Phys. **67**, 781 (1995).

[10] Y. Totsuka (SuperKamiokande Collaboration), in the Proceedings of the 35th International School of Subnuclear Physics (Erice, Italy, 1997), to appear.

[11] G. L. Fogli, E. Lisi and D. Montanino, University of Bari Report No. BARI-TH/284-97, hep-ph/9709473, to appear in Astropart. Phys.

[12] N. Hata and P. Langacker, Phys. Rev. D **56**, 6107 (1997).

[13] Borexino Collaboration, C. Arpesella *et al.*, "INFN Borexino proposal," Vols. I and II, edited by G. Bellini, R. Raghavan, *et al.* (University of Milan, 1992); J. Benziger, F. P. Calaprice *et al.*, "Proposal for Participation in the Borexino Solar Neutrino Experiment," (Princeton University, 1996).

[14] Updated information about the Borexino experiment can be found at the URL http://almime.mi.infn.it .

[15] Borexino Collaboration, G. Bellini *et al.* in *TAUP '95*, Proceedings of the 4th International Workshop on Theoretical and Phenomenological Aspects of Underground Physics, Toledo, Spain, edited by A. Morales, J. Morales, and J. A. Villar [Nucl. Phys. (Proc. Suppl.) **B48**, 547 (1996)], p. 363; G. Bellini, in *La Thuile '97*, Proceedings of the 11th Rencontres de Physique de la Vallée d'Aoste, La Thuile, Italy, 1997, ed. by M. Greco (Frascati Physics Series, Vol. 9), p. 27.

[16] R. S. Raghavan, Science **267**, 45 (1995).

[17] J. N. Bahcall and P. I. Krastev, Phys. Rev. C **55**, 929 (1997).

[18] K. Lande (Homestake Collaboration), in *ν4*, Proceedings of the 4th International Solar Neutrino Conference, Heidelberg, Germany, 1997, ed by W. Hampel (Max Planck Institute, Heidelberg, 1998), p. 85.

[19] V. N. Gavrin (SAGE Collaboration), in *News about SNU's*, International Workshop on Solar Neutrinos (Institute of Theoretical Physics, Santa Barbara, CA, 1997). Proceedings available at the URL http://www.itp.ucsb.edu/online/snu .

[20] W. Hampel (GALLEX Collaboration), in *News about SNU's* [19].

[21] G. L. Fogli and E. Lisi, Astropart. Phys. **3**, 185 (1995).

[22] J. N. Bahcall, P. I. Krastev, and E. Lisi, Phys. Rev. C **55**, 494 (1997).

[23] B. Faïd, G. L. Fogli, E. Lisi and D. Montanino, Phys. Rev. D **55**, 1353 (1997).

[24] S. P. Mikheyev and A. Yu. Smirnov, ICTP Report No. IC-97-113, hep-ph/9708403.

[25] G. L. Fogli, E. Lisi and D. Montanino, Phys. Rev. D **56**, 4374 (1997).

[26] G. L. Fogli, E. Lisi and D. Montanino, University of Bari Report No. BARI-TH/296-98, hep-ph/9803309, submitted to Phys. Lett. B.

[27] M. Nakahata, in *P4 '97*, Proceedings of the APCPT Pacific Particle Physics Phenomenology Conference, (Seoul, Korea, 1997); also available at the URL http://www-sk.icrr.u-tokyo.ac.jp/doc/sk/pub∼.

[28] K. Inoue, in *TAUP '97*, Proceedings of the 5th International Workshop on Topics in AstroParticle and Underground Physics (Gran Sasso, Italy, 1997), to appear in Nucl. Phys. B (Proc. Suppl.); also available at the same URL as in ref. [27].

[29] Y. Suzuki, in *Neutrinos in Astro, Particle and Nuclear Physics*, Proceedings of the 19th International School of Nuclear Physics (Erice, Italy, 1997), to appear; also available at the same URL as ref. [27].

[30] Y. Itow, in the Proceedings of the Topical Conference "Physics of Leptons," SLAC Summer Institute 1997; (Stanford, CA, 1997), to appear; also available at the same URL as ref. [27].

[31] H. Sobel, in the Proceedings of the Aspen Winter Conference on Particle Physics: Frontiers in Particle Physics (Aspen, CO, 1998), to appear.

[32] I. Pomeranchuk, as cited in Gribov and Pontecorvo [1].

[33] G. L. Fogli, E. Lisi, D. Montanino, and G. Scioscia, Phys. Rev. D **56**, 4365 (1997).

[34] J. N. Bahcall, M. Kamionkowsky, and A. Sirlin, Phys. Rev. D **51**, 6146 (1995).

# FIGURES

FIG. 1. Vacuum oscillation solutions to the solar neutrino deficit in the usual mass-mixing plane, as derived from a fit to the data of Table I. The four regions A, B, C, and D, are allowed at 95% C.L.

FIG. 2. Energy spectrum of recoil electrons in Borexino. The main components are shown separately. The smearing effect of the energy resolution is also shown. The arrows indicate the prospective energy window assumed in the analysis.

FIG. 3. SuperKamiokande (SK) experiment. Map of the four vacuum oscillation solutions A, B, C, and D in the plane charted by $\Delta\langle T\rangle/\langle T\rangle$ (the fractional deviation of the mean electron kinetic energy) and by $f_1-\varepsilon$ (the deviation of the first Fourier component from its standard value). Notice the strong correlation between these two variables, which is induced by the $L/E$ dependence of the oscillation probability. The star at the origin corresponds to the standard (no oscillation) case. The SuperKamiokande datum on $\Delta\langle T\rangle/\langle T\rangle$ is also shown; it disfavors solution C at $> 4\sigma$ and solution D at $> 6\sigma$. The part of the solution $A$ which is favored by the SK datum at $1\sigma$ corresponds to an expected Fourier amplitude $f_1 - \varepsilon \simeq 0.5$–1%.

FIG. 4. Borexino (BX) experiment. Map of the four vacuum oscillation solutions A, B, C, and D, in the plane charted by the first two Fourier components. The star at the origin corresponds to the no oscillation case. There is some overlap among the four solutions.

FIG. 5. SuperKamiokande (SK) *vs* Borexino (BX). Map of the four vacuum oscillation solutions A, B, C, and D in the planes charted by the SK observables $\Delta\langle T\rangle/\langle T\rangle$ and $f_1 - \varepsilon$ (ordinates) and by the BX observables $f_1 - \varepsilon$ and $f_2$ (abscissae). Future measurements of the $f_n$'s in SK and BX, together with increasingly accurate $\Delta\langle T\rangle/\langle T\rangle$ data from SK, are expected to spot one of the solutions.

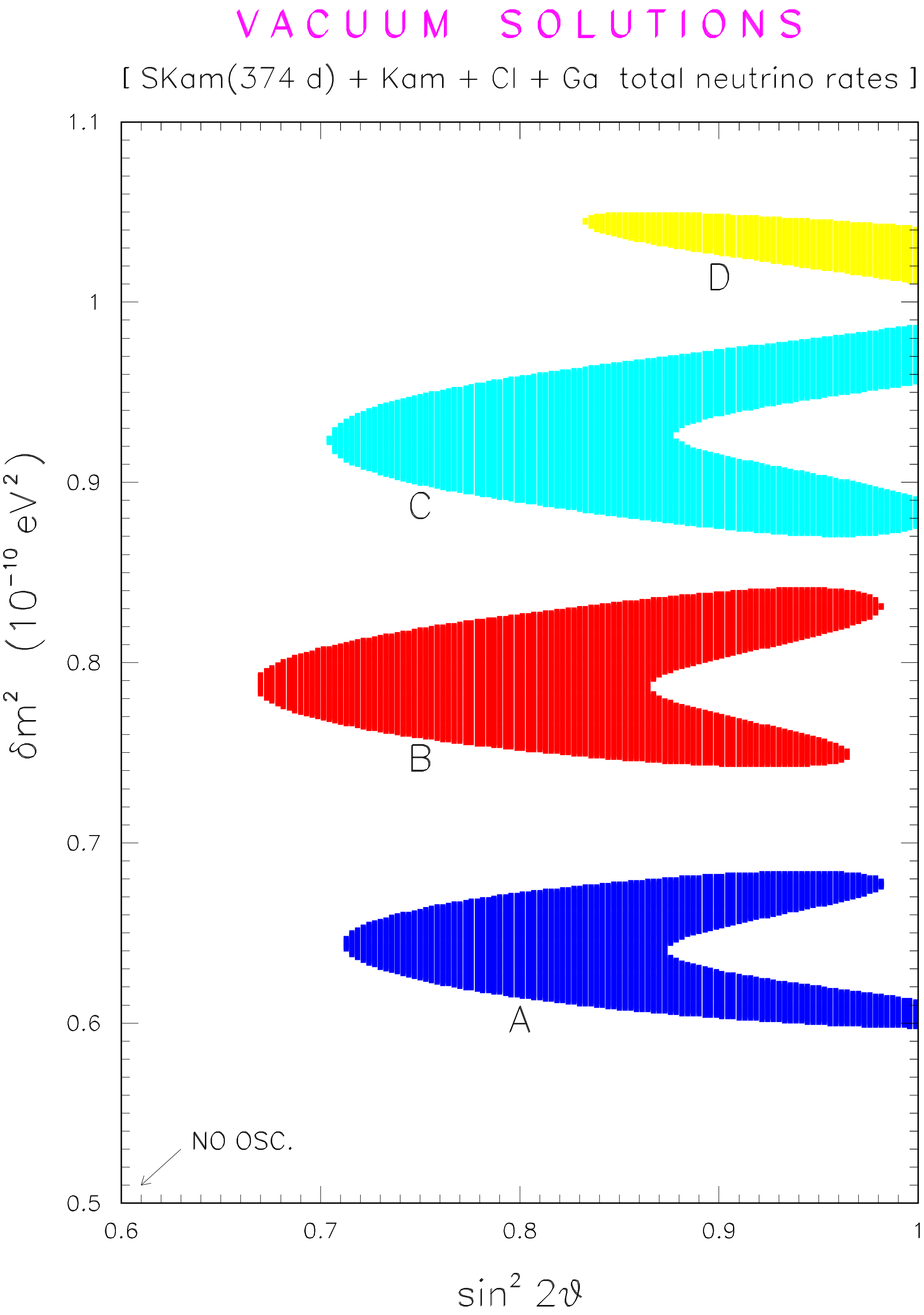

FIG. 1. Vacuum oscillation solutions to the solar neutrino deficit in the usual mass-mixing plane, as derived from a fit to the data of Table I. The four regions A, B, C, and D, are allowed at 95% C.L.

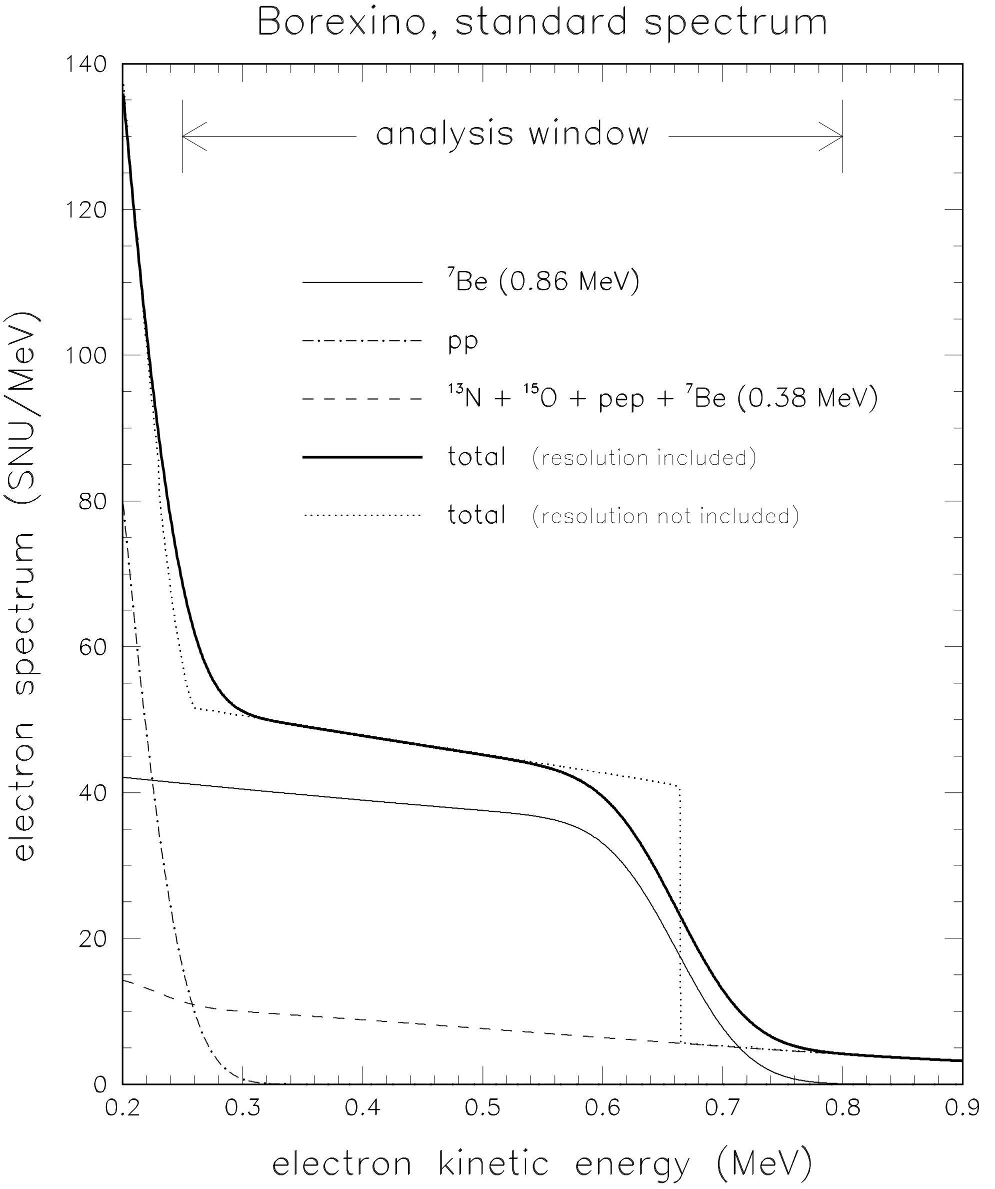

FIG. 2. Energy spectrum of recoil electrons in Borexino. The main components are shown separately. The smearing effect of the energy resolution is also shown. The arrows indicate the prospective energy window assumed in the analysis.

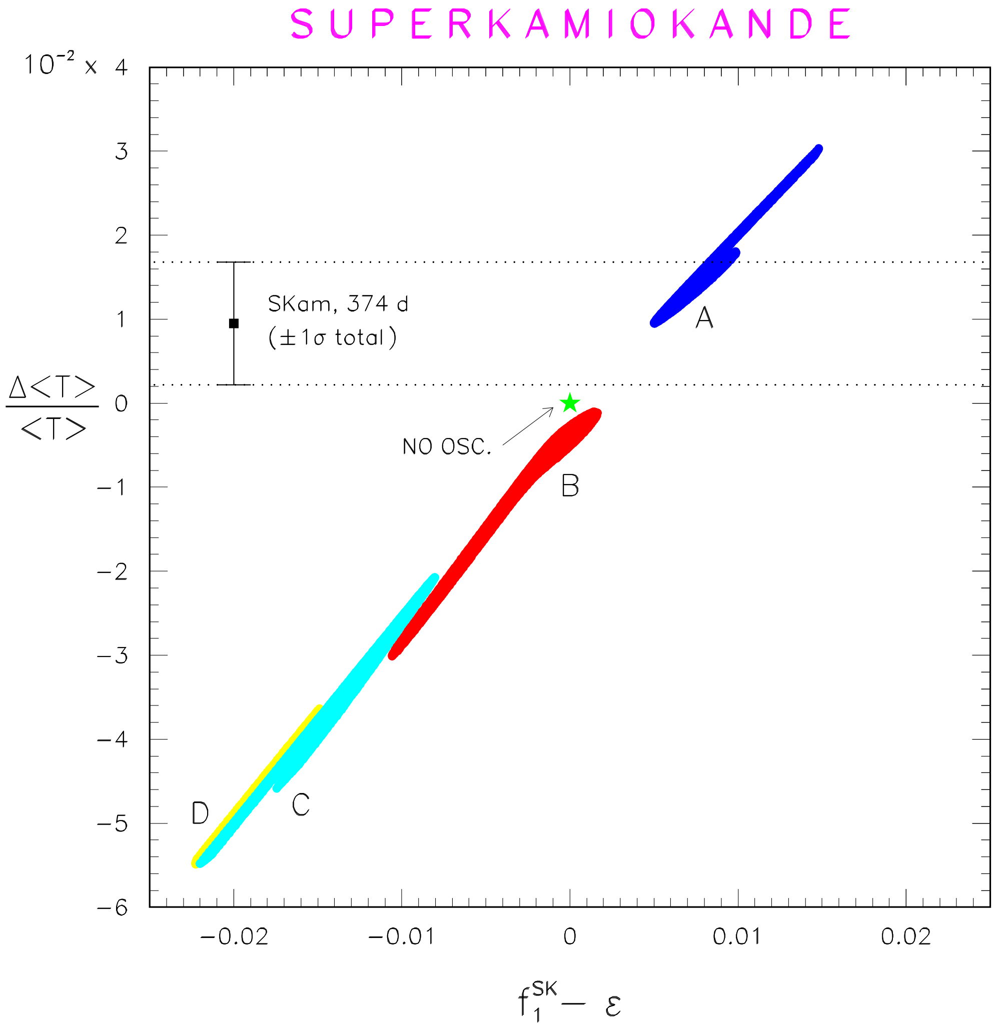

FIG. 3. SuperKamiokande (SK) experiment. Map of the four vacuum oscillation solutions A, B, C, and D in the plane charted by $\Delta\langle T\rangle/\langle T\rangle$ (the fractional deviation of the mean electron kinetic energy) and by $f_1-\varepsilon$ (the deviation of the first Fourier component from its standard value). Notice the strong correlation between these two variables, which is induced by the $L/E$ dependence of the oscillation probability. The star at the origin corresponds to the standard (no oscillation) case. The SuperKamiokande datum on $\Delta\langle T\rangle/\langle T\rangle$ is also shown; it disfavors solution C at $> 4\sigma$ and solution D at $> 6\sigma$. The part of the solution $A$ which is favored by the SK datum at $1\sigma$ corresponds to an expected Fourier amplitude $f_1 - \varepsilon \simeq 0.5$–1%.

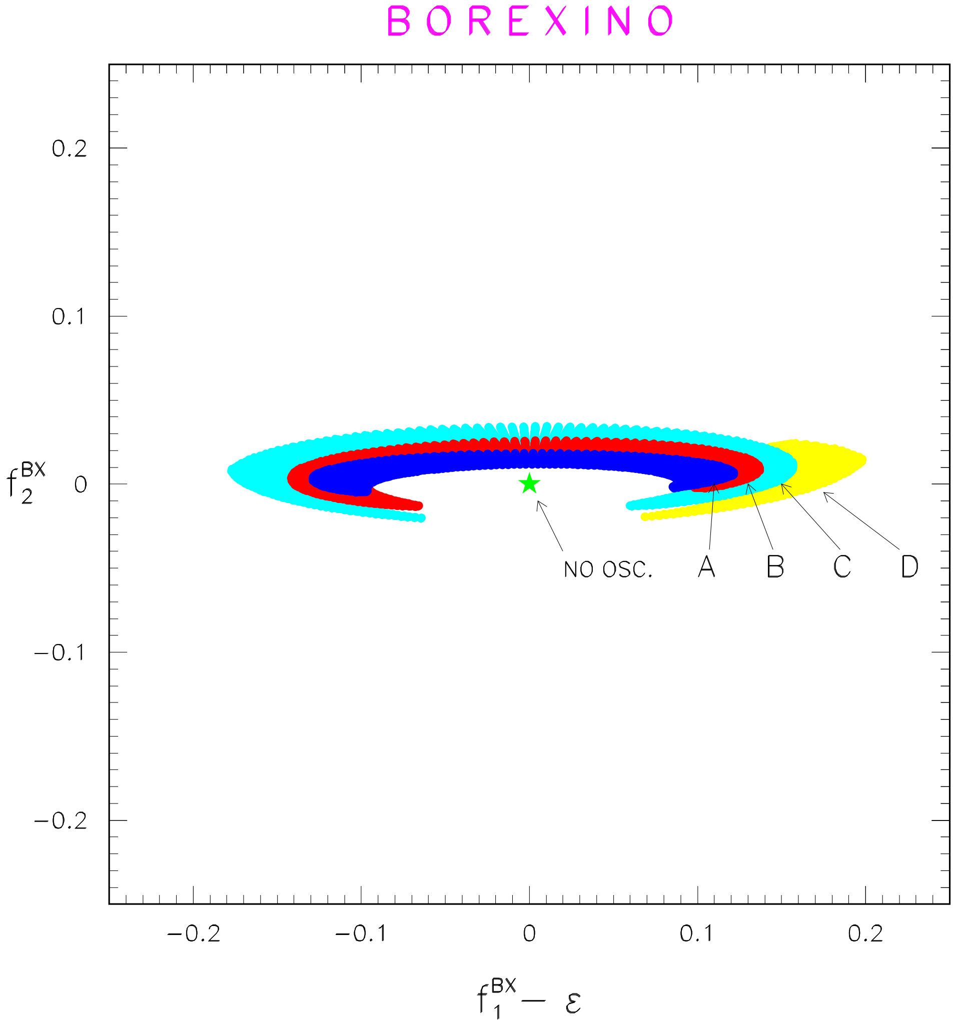

FIG. 4. Borexino (BX) experiment. Map of the four vacuum oscillation solutions A, B, C, and D, in the plane charted by the first two Fourier components. The star at the origin corresponds to the no oscillation case. There is some overlap among the four solutions.

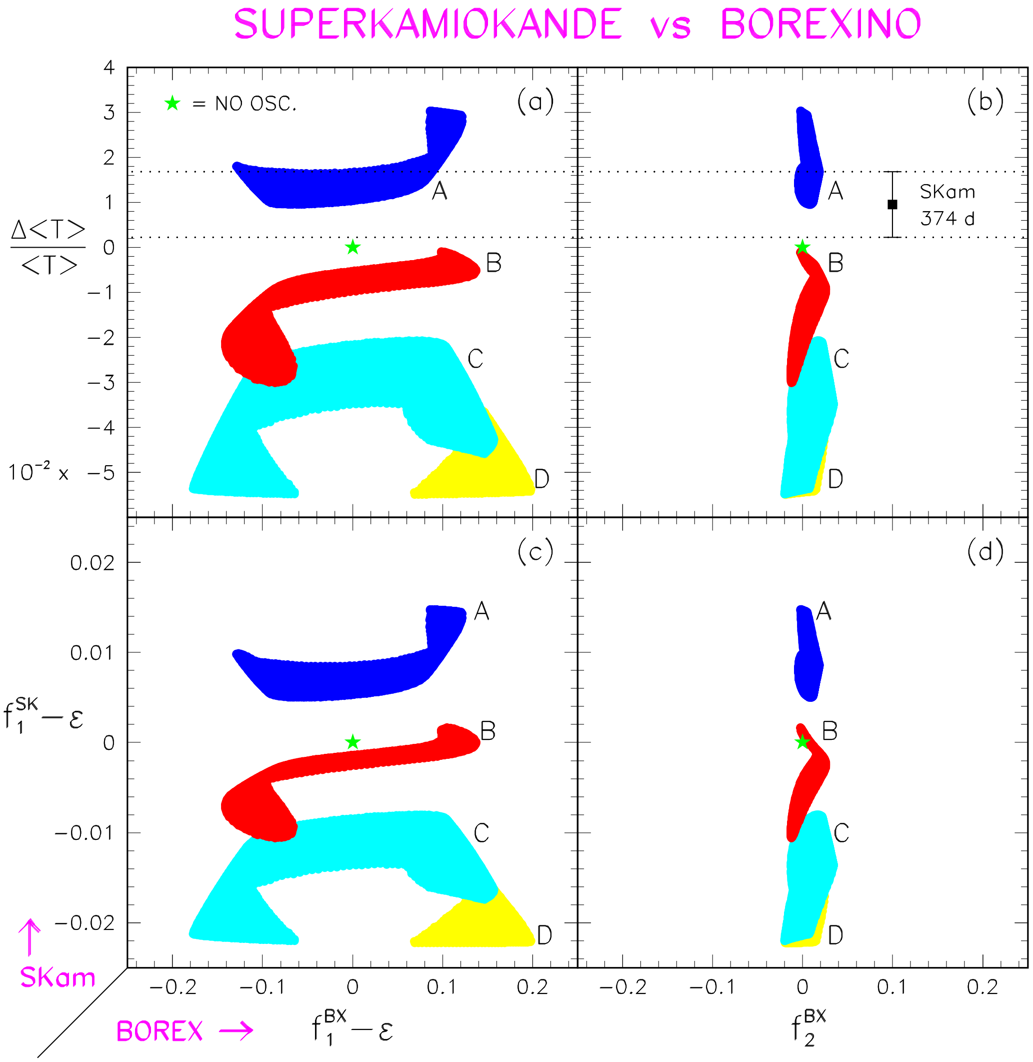

FIG. 5. SuperKamiokande (SK) *vs* Borexino (BX). Map of the four vacuum oscillation solutions A, B, C, and D in the planes charted by the SK observables $\Delta\langle T\rangle/\langle T\rangle$ and $f_1 - \varepsilon$ (ordinates) and by the BX observables $f_1 - \varepsilon$ and $f_2$ (abscissae). Future measurements of the $f_n$'s in SK and BX, together with increasingly accurate $\Delta\langle T\rangle/\langle T\rangle$ data from SK, are expected to spot one of the solutions.